

The Fundamental Plane of Black Hole Activity in the Optical Band

Payaswini Saikia^{1*}, Elmar Körding¹ and Heino Falcke^{1,2,3}

¹*Department of Astrophysics/IMAPP, Radboud University, Nijmegen, P.O. Box 9010, 6500 GL Nijmegen, The Netherlands*

²*ASTRON, Oude Hoogeveensedijk 4, 7991 PD Dwingeloo, The Netherlands*

³*Max-Planck-Institut für Radioastronomie, auf dem Hügel 69, 53121 Bonn, Germany*

Received: 2015 March 25. Accepted: 2015 March 30.

ABSTRACT

Black hole accretion and jet formation have long been thought to be scale invariant. One empirical relation suggesting scale invariance is the Fundamental Plane of Black Hole activity, which is a plane in the space given by black hole mass and the radio/X-ray luminosities. We search for an alternative version of this plane using the luminosity of [OIII] emission line instead of X-ray luminosity. We use a complete sample of 39 supermassive black holes selected from the Palomar Spectroscopic Survey with available radio and optical measurements and information on black hole mass. A sample of stellar mass X-ray binaries has also been included to examine if physical processes behind accretion is universal across the entire range of black hole mass. We present the results of multivariate regression analysis performed on the AGN sample and show that the sample stretches out as a plane in the 3D logarithmic space created by bolometric luminosity, radio luminosity and black hole mass. We reproduce the established Fundamental Plane of Black Hole activity in X-rays. We show that this plane can be obtained with the supermassive black hole sample alone and the X-ray binaries agrees to the found relation. We also discuss radio loudness of various classes of low-luminosity AGN in view of our fundamental plane.

Key words: galaxies: active; fundamental plane; galaxies: nuclei

1 INTRODUCTION

Accretion physics is thought to scale globally across black holes of different mass scale – from millions of solar masses Supermassive black holes (SMBH) to ~ 10 solar masses stellar X-ray binaries (XRBs).

Many theoretical arguments and observational evidences have been put forward to support scale-invariance of black hole accretion and relativistic jet physics. The amount of synchrotron radiation emitted from a scale invariant jet is theoretically shown to depend both on the black hole mass and the accretion rate (eg. Falcke & Biermann 1995; Heinz & Sunayev 2003). The observational evidence supporting the same is the fundamental plane of black hole activity connecting XRBs and AGN. It is a non-linear empirical correlation in the space given by the black hole mass, the radio luminosity and the X-ray luminosity with high statistical significance (Merloni et al. 2003; Falcke et al. 2004). The radio luminosity is used in the fundamental plane relation as a probe for the AGN jet (Blandford & Königl 1979) while the X-ray emission is taken to be a tracer for accretion rate.

In this study, we use the forbidden [OIII] emission line luminosity as an indirect tracer of accretion rate instead of X-ray luminosity and re-establish the fundamental plane relation for black hole activity. Generally, X-ray luminosity is a better proxy for the bolometric luminosity and accretion rate, but they are costly to obtain and hence are not easily available. The [OIII] luminosity, on the other hand, can be measured by ground-based observations and hence is easily available. In addition, as the Narrow Line Region extends far beyond the central source, torus obscuration of the [OIII] emission line is minimized compared to X-ray emission. Moreover, spectral index variations are less of an issue while using the [OIII] line luminosity. In general, [OIII] lines are strong, easy to detect and are known to be relatively weak in metal-rich, star-forming galaxies. Hence, the emission line [OIII] $\lambda 5007$ ($2s^2 2p^2 \ ^1D_2 - 2s^2 2p^2 \ ^3P_2$) is commonly used as a surrogate for the bolometric luminosity (eg. Heckman et al. 2004; Falcke et al. 1995) and as a tracer of the nuclear luminosity (eg. Kauffmann et al. 2003). Using this [OIII] emission line luminosity as a proxy for the accretion rate and the 15 GHz radio luminosity as the tracer for jet emission, we have examined the disc-jet connection in black holes of different masses by investigating their correlations.

* E-mail: p.saikia@astro.ru.nl

Later we convert the [OIII] luminosities of the supermassive black holes to X-ray and Bolometric luminosities in order to compare them with the smaller mass X-ray binaries.

We use a complete sample of 39 supermassive black holes and a selected sample of the best-studied stellar mass X-ray binaries for this work. The sample is described in Section 2. In Section 3, we present multivariate regression analysis results of the supermassive black hole plane in [OIII]. We reproduce the fundamental plane of black hole activity in Section 4 and introduce the bolometric fundamental plane in Section 5. Finally in Section 6, we discuss our results and present the conclusions of this study in Section 7.

2 SAMPLE SELECTION

2.1 Supermassive black holes

To study the general properties of accretion, it is preferred to have a complete sample of galaxies covering a broad range of spectral types, luminosities and morphological types. For the entire sample, information on velocity dispersion, radio luminosity and [OIII] line luminosity are required to estimate the black hole mass, jet emission and accretion rate respectively. The best currently available complete sample in the northern hemisphere is the Palomar Spectroscopic Survey (Ho et al. 1995), comprising the nuclear region of 486 nearby galaxies with $B_r < 12.5$ mag. The SMBH sample used for this study has been extracted from this Palomar Survey and hence is mainly targeted on the low-luminosity AGN.

Several multi-wavelength surveys have been performed on the Palomar Sample. Radio luminosities for this study, which are needed as an estimate for the jet emission, have been taken from the high resolution radio survey of all LLAGNs and AGNs in the Palomar sample, presented by Nagar et al. (2005). From the Palomar survey, Nagar et al. (2005) selects all 403 galaxies with nuclear emission lines - 206 of these nuclei have H II region type spectra, and the rest 197 are the AGN. They report 197 VLA 15 GHz and 44 VLBI 5 GHz flux measurements. For this analysis, we need the nuclear radio luminosity and hence we need the flat-spectrum radio cores in our galaxies. Therefore, we use only the VLA data as the VLA survey gives higher frequency luminosities and hence is designed to pick up galaxies with a flat spectrum radio core.

The [OIII] line luminosities, used in the study as a tracer of the accretion rate, have been taken from Ho et al. (1997), where spectroscopic properties and parameters for 418 AGN and their host galaxies are presented. It is important to note that the [OIII] emission line can be attenuated by dust within the host galaxy. The observed [OIII] luminosity can be corrected for this extinction by using the Balmer decrement

$$L_{OIII}^c = L_{OIII} \left(\frac{(H\alpha/H\beta)_{obs}}{3.0} \right)^{2.94}, \quad (1)$$

where the intrinsic Balmer decrement is taken to be 3.0 (eg. Osterbrock & Ferland 2006). The black hole mass estimate can be obtained through the established empirical relation between black hole mass and central stellar velocity dispersions. For this study, we use the stellar velocity dispersions presented in Ho et al. (2009) to derive the black

hole masses. These velocity dispersions are calculated using the same spectra. The equation we use to determine mass from velocity dispersion is (McConnell et al. 2011)

$$\log \frac{M_{BH}}{M_\odot} = 8.29 + 5.12 \log_{10} \frac{\sigma}{200 \text{ km/s}}. \quad (2)$$

We restrict our final sample to the galaxies which have available data in 15 GHz radio luminosity, [OIII] emission line luminosity and black hole mass; yielding a sample of 101 galaxies. This restriction introduces observational bias in the sample. In order to properly constrain the parameters of the proposed correlation, we exclude the upper limits from our final dataset. We later perform partial Kendall τ correlation test to check for the significance of the plane and find that the underlying correlation exists even in the presence of the upper limits.

Removing the upper limits reduces the sample size to 39 supermassive black holes, comprising 20 LINERS, 12 Seyferts and 7 Transition galaxies. The final sample can be morphologically classified as 7 Ellipticals, 18 Spirals, 1 Irregular and 13 Lenticulars. This is the complete sample of AGN from the optically-selected Palomar survey of all northern galaxies, showing AGN-like spectra and having detected radio and [OIII] line luminosities.

2.2 Stellar black holes

A homogeneous sample of black holes covering the entire black hole mass range is required to study general properties of accretion. Hence, we include stellar mass galactic black holes to our sample of supermassive black holes. Stellar mass XRBs are classified into different states according to their accretion - the low hard, the high soft and the intermediate states (Remillard & McClintock 2006). The radio spectrum in the low/hard state is consistent with the spectra of a steady jet (Fender et al. 2004) while radio emission seems to be quenched in the high/soft state (Fender et al. 1999; Corbel et al. 2000).

X-ray Binaries in the low/hard state follow a universal correlation between the radio and X-ray luminosity of the form $L_R \propto L_X^{0.7}$ (Gallo et al. 2003), dominated by the observations of GX 339-4 and V404 Cyg. For our study, we take a selected sample of the best-studied X-ray Binaries in the hard state. This study does not use the 'radio-quiet' XRBs forming the outlier track of the universal radio/X-ray correlation (eg. Coriat et al. 2011; Gallo et al. 2012, etc.).

GX 339-4: Data presented in Corbel et al. (2013) as 88 quasi-simultaneous radio and X-ray observation from a long-term campaign of GX 339-4 in the low/hard state, has been used for this study. GX 339-4 is believed to have a black hole with a mass $> 5.8 M_\odot$ (Hynes et al. 2003). The distance to GX 339-4 is taken to be 8 Kpc (Zdziarski et al. 2004).

V404 Cyg: We use the VLA radio and *Chandra* X-ray observations of V404 Cyg in the hard state, as reported in Corbel et al. (2008) for this study. The distance to this source is taken to be 3.5 Kpc (Zycki et al. 1999) while the black hole mass is taken as $10 M_\odot$ (Shahbaz et al. 1996).

XTE J1118+480: The X-Ray transient XTE J1118+480 at it's hard state is also included in the XRB sample. The radio and X-ray luminosities are directly taken from the compilation in Merloni et al. (2003).

A0620-00: Finally, we also include the simultaneous *Chandra* X-ray and VLA radio observation of A06200-00 in the hard state, as reported in Gallo et al. (2006). This source has a black hole of mass $11.0 \pm 1.9 M_{\odot}$ (Gelino et al. 2001) and lies at a distance of 1.2 ± 0.4 Kpc (Shahbaz et al. 1994; Jonker & Nelemans 2004).

3 FUNDAMENTAL PLANE IN [OIII]

The final sample of supermassive black holes stretches out in a plane in the three-dimensional logarithmic space defined by the 15 GHz radio luminosity, [OIII] line luminosity and black hole mass. The resulting plane is obtained with some scatter owing to various measurement errors and intrinsic variability of sources.

3.1 Multivariate Regression Analysis

We perform a Multivariate Correlation Linear regression analysis on the data to estimate the parameters for the plane. Standard chi-square fits used for analysis yield asymmetric results as it can not consider the scatter in all variables (eg. Fasano & Vio 1998). Hence, we use the modified chi-square estimator known as merit function, as uncertainties are present in all the required measurements. The merit function is defined as

$$\chi^2(a, b) = \sum_i \frac{(y_i - b - \sum_j a_j x_{ij})^2}{\sigma_{yi}^2 + \sum_j (a_j \sigma_{xij})^2}, \quad (3)$$

where $\sigma_{x_{ij}}$ and σ_{y_i} are the respective uncertainties. Here y_i denotes the [OIII] line luminosities, x_{1j} the radio luminosities at 15 GHz and x_{2j} the black hole masses. The linear regression coefficients a_j and the zero intercept b are the unknown parameters that can be found by minimizing χ^2 .

It is not possible to minimize the merit function analytically as the equation is nonlinear in a_j . But we can analytically solve for the constant b and then a simple numerical optimization routine can be used to find the parameter a_j s.

3.2 Error budget

To correctly extract the parameters of the plane, it is crucial to estimate the errors cautiously for each variable. It has been observed that the resulting parameters of the fundamental plane correlation depend strongly on the choices of assumed uncertainties in the data (Körding et al. 2006).

Uncertainty in luminosity depends on both flux and distance measurements. Errors in radio and optical fluxes are different for each data point, and are usually very low - less than 10%. For this analysis, we use a typical value of 0.05 dex as the uncertainty in flux. Errors in distance measurement typically range from 0.1 to 0.4 dex. We adopt an uniform value of 0.15 dex for our distance uncertainty.

In addition to these, we include an intrinsic scatter term whose exact magnitude is chosen to ensure that the reduced merit function is unity. For the SMBH plane, we get an intrinsic scatter of 0.35dex. It gets further reduced to 0.2 dex for the combined plane obtained with the complete black hole sample of SMBH and XRBs. This scatter term takes into account various factors like source peculiarities,

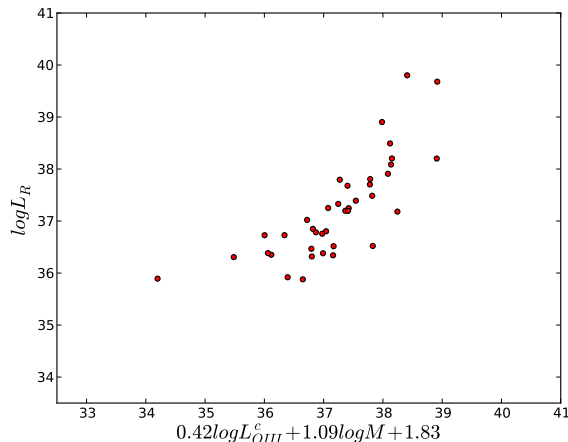


Figure 1. Projection of the Optical Fundamental Plane with Supermassive Black Holes. Luminosities are given in erg/s while the masses are in the unit of solar mass.

non-simultaneous measurements of radio and optical flux of AGN, effects of spin, beaming statistics, absorption etc.

We estimate the SMBH masses from the available velocity dispersions using the M - σ relation. Merritt & Ferrarese (2001) give an absolute scatter of 0.34 dex for this relation, which can be used as a measure of the uncertainty for the SMBH mass estimate.

3.3 Correlation Tests

We perform the Kendall Tau Correlation Test on our SMBH sample to statistically verify the significance of the plane. The Kendall tau value is a measure of the correlation between the specified measurements. For the L_R - L_{OIII} - M plane defined by the sample, we get a Kendall Tau coefficient value of $\tau = 0.67$ (with the probability for null hypothesis as $P_{null} \simeq 1.3 \times 10^{-9}$). For the plane obtained with extinction-corrected [OIII] luminosities (see Fig 1), we obtain $\tau = 0.66$ (with $P_{null} \simeq 2.8 \times 10^{-9}$).

It is also important to statistically check for spurious effects in Luminosity-Luminosity plots due to their common dependence on distance. Kendall Tau Partial Correlation analysis was performed with distance as the third variable. The correlation was found to be real even after taking into account the large range of distance ($\tau = 0.48$, with $P_{null} \simeq 3.9 \times 10^{-3}$).

As mentioned, the sample size substantially increases from 39 to 101 galaxies, if upper limits are included in the dataset. In order to assess the significance of the apparent correlations in the presence of upper limits, we have adopted the method proposed by Akritas & Siebert (1996), using which a Partial Kendall Tau correlation test can be performed in the presence of censored data. Applying this test to our data, we find a Partial Kendall τ value of 0.36 (with $P_{null} \simeq 4.4 \times 10^{-12}$) showing that although the significance of the plane reduces while taking into account the upper limit data, a real underlying correlation indeed exists.

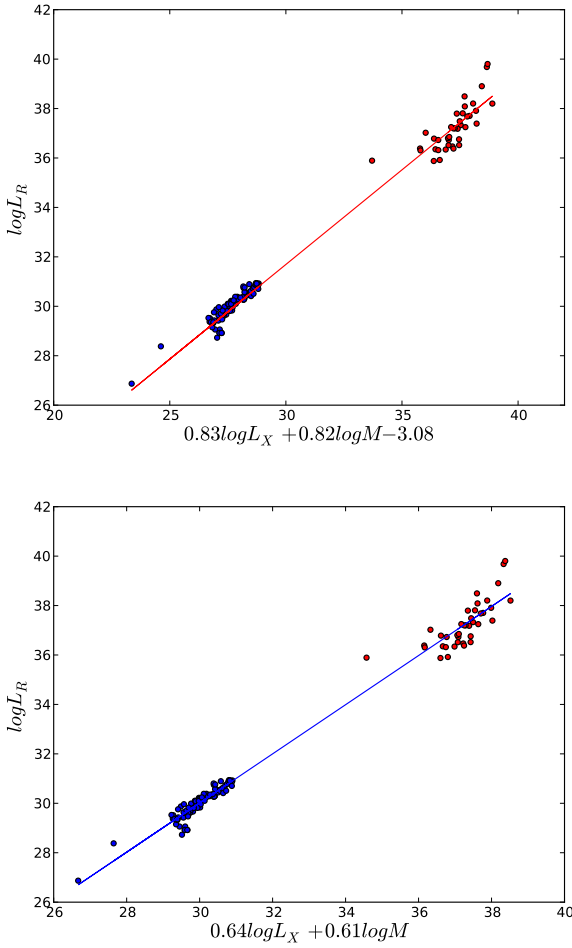


Figure 2. Projection of the Fundamental Plane. In the top plot, SMBH sample is shown in red with the red solid line depicting the best-fit line for the SMBH sample. The XRB sample is put on the graph as blue dots without fitting. In the bottom plot, we show the combined fit for the complete sample including both the SMBH and the XRB sample. The blue line is the obtained best-fit line. Luminosities are given in erg/s while the masses are in the unit of solar mass.

3.4 Results

After statistically verifying the significance of the plane, we use the merit function to estimate the plane equation. We obtain the best fit coefficients for the function

$$\log L_R = \xi_{RO} \log L_{OIII}^c + \xi_{RM} \log M + b_R,$$

where ξ_{RO} and ξ_{RM} denote the respective correlation indices and b_R is the constant offset.

We perform the multivariate regression analysis on the complete sample of SMBH using [OIII] line luminosity as an estimate of mass accretion, and obtain the best fit plane described by

$$\log L_R = (0.83 \pm 0.4) \log L_{OIII} + (0.82 \pm 0.3) \log M.$$

On the other hand, using the extinction-corrected [OIII] luminosities, we get a plane with different parameters

$$\log L_R = (0.42 \pm 0.15) \log L_{OIII}^c + (1.09 \pm 0.22) \log M$$

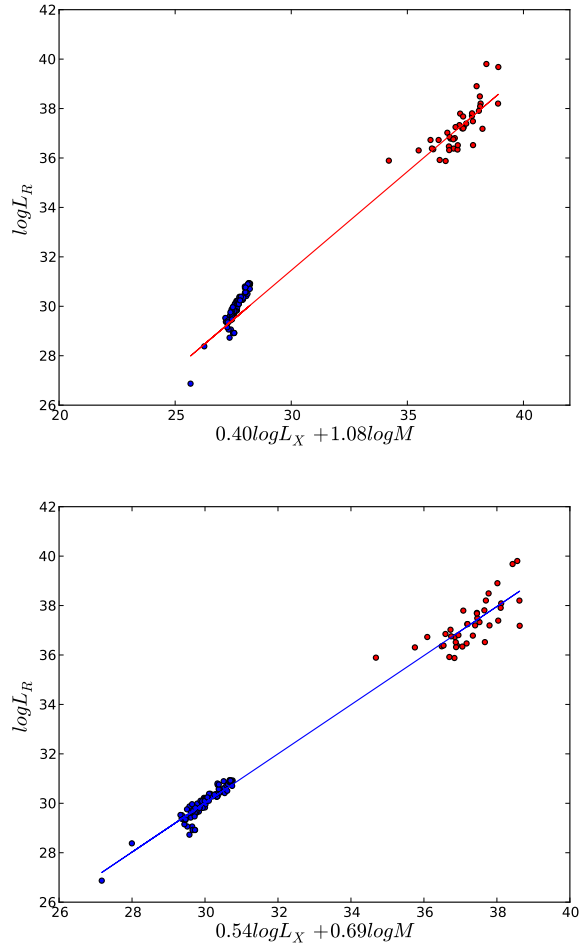


Figure 3. Same as Fig 2, but with X-ray luminosity obtained from the relation proposed by L09.

4 REPRODUCING THE FUNDAMENTAL PLANE IN X-RAYS

To reproduce the established Fundamental Plane of Black Hole activity (Merloni et al. 2003; Falcke et al. 2004) we have included XRB data to our sample. The fundamental plane of black hole activity is a plane in the space given by black hole mass and the radio/X-ray luminosities, in the form of

$$\log L_R = \xi_{RX} \log L_X + \xi_{RM} \log M + b_R.$$

4.1 Using observed [OIII] luminosity

The SMBH [OIII] emission line luminosity is converted to X-ray luminosity with the relation proposed by Heckman et al. (2005) (hereafter H05), which states that the hard X-ray (3-20 keV) and [OIII] line luminosities are well-correlated with the mean value for $\log (L_{3-20\text{keV}}/L_{OIII})$ as 2.15 dex.

As the X-ray range used for our study is 2-10 keV, it is required to modify the Heckman relation of $L_{3-20\text{keV}}/L_{OIII}$ to a correlation between luminosities of 2-10 keV and luminosities of [OIII] emission line to ensure consistency.

To find the needed correlation, we use the hard X-ray selected sample of 47 local AGN used in H05. For 23 of

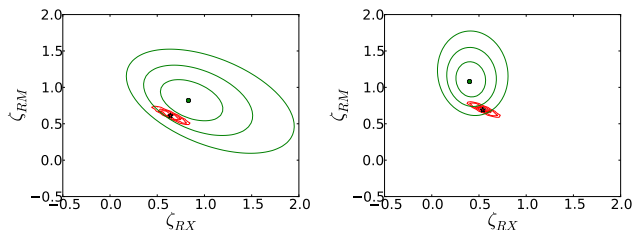


Figure 4. χ^2 confidence ellipses for the observed correlation coefficients ξ_{RX} and ξ_{RM} , depicting 1, 2 and 3 sigma confidence levels (Green - only SMBH, Red - both SMBH and XRB). The first plot is for X-ray luminosity obtained from Heckman relation, while the second one is for Lamastra-obtained X-ray luminosity.

these galaxies, 2-10 keV luminosities are provided in H05. 12 more galaxies of the sample have their 2-10keV range luminosities recorded in CAIXA - XMM Newton catalogue (Bianchi et al. 2009). We compile the luminosities in 2-10 keV range for the complete sample, whenever available. As the photoelectric absorption effects are more significant in the 2-10 keV band compared to the 3-20 keV specially for the Type 2 AGNs which can have high absorbing column densities, we exclude them from the sample. We investigate the correlation of the X-ray (2-10 keV) and [OIII] line luminosities for the Type 1 AGNs of the sample and find the mean value for $\log(L_{2-10\text{KeV}}/L_{\text{OIII}})$ as 1.81 dex. With this conversion factor, we estimate the luminosity of our SMBH sample at 2-10 keV range.

We first fit only the supermassive black hole sample and obtain a relation

$$\log L_R = (0.83 \pm 0.3) \log L_X + (0.82 \pm 0.2) \log M - 3.08 .$$

Extrapolating this relation to lower black hole masses and putting the XRB data in the plot without fitting it, we find that the stellar mass black hole are consistent with the plane found with only the supermassive black holes (see Fig 2). Fitting the XRBs along with the SMBH sample yield results that are in agreement with the relation found with only SMBH, within the errors. This combined fit results in a plane defined by the parameters $\xi_{RX} = 0.64 \pm 0.4$ and $\xi_{RM} = 0.61 \pm 0.2$.

This plane is also in agreement with the fundamental plane of black hole activity reported in previous studies. For a sample consisting of XRBs, SgrA, LLAGN, Seyferts and Transitions galaxies, Körding et al. (2006) has reported the plane parameters as $\xi_{RX} = 0.53 \pm 0.10$ and $\xi_{RM} = 0.71 \pm 0.19$, while Merloni et al. (2003) reports their plane parameters after taking high-state objects into account as $\xi_{RX} = 0.60 \pm 0.11$ and $\xi_{RM} = 0.78 \pm 0.10$.

4.2 Using extinction-corrected [OIII] luminosity

Lamastra et al. (2009) (hereafter L09) also investigates for a correlation between [OIII] and X-ray luminosities, but unlike H05 they use extinction-corrected [OIII] line luminosities. They report a linear correlation between L_X and L_{OIII}^c , which is given by

$$\log \frac{L_X}{10^{42} \text{erg/s}} = (1.11 \pm 0.10) + (1.02 \pm 0.06) \log \frac{L_{\text{OIII}}^c}{10^{42} \text{erg/s}} .$$

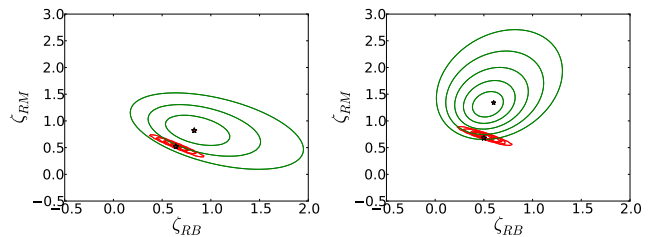


Figure 5. χ^2 confidence ellipses for the observed correlation coefficients ξ_{RB} and ξ_{RM} of the Bolometric fundamental planes (Green - only SMBH, Red - both SMBH and XRB), depicting 1, 2 and 3 sigma confidence levels. The first plot is for X-ray luminosity obtained from Heckman relation, while the second one is for Lamastra-obtained X-ray luminosity.

We see that the correlation coefficients of the plane changes considerably when extinction-corrected [OIII] luminosities are used to obtain the X-ray luminosities. We obtain the best fit coefficients as $\xi_{RX} = 0.40 \pm 0.15$ and $\xi_{RM} = 1.08 \pm 0.22$ for the SMBH sample only, and $\xi_{RX} = 0.54 \pm 0.1$ and $\xi_{RM} = 0.69 \pm 0.1$ for the combined fitting of the SMBH and the XRB sample, yielding a plane defined by

$$\log L_R = (0.54 \pm 0.1) \log L_X + (0.69 \pm 0.1) \log M .$$

As seen by the bootstrapping error range and chi-square maps (see Fig 4), the fundamental plane obtained from SMBH using extinction-corrected [OIII] luminosities is better-constrained. But strangely in this case the stellar mass black hole data do not agree completely to the fit obtained only with the SMBH sample, although a combined fit of the complete sample does reproduce the fundamental plane. The plots can be seen in Fig 3.

In Fig 4, we show our results as χ^2 confidence ellipses traced out by variation of c in the (a, b) parameter space. The model used has two degrees of freedom and hence the 1σ confidence region is given by $\Delta\chi^2 = 2.3$. Similarly, $\Delta\chi^2 = 6.18$ and $\Delta\chi^2 = 11.83$ represent the 2σ and 3σ confidence regions, respectively. Here, the contours represent 1, 2 and 3 sigma confidence levels. As shown in the χ^2 confidence maps, while the parameters obtained from fitting only the SMBH gives us a 3σ result, the combined fit of the complete sample including both SMBH and XRB gives much better constrained parameters.

5 BOLOMETRIC FUNDAMENTAL PLANE

To compare the X-ray binaries to our sample of SMBHs, bolometric luminosity can also be used as the estimate for accretion rate. The relation then becomes

$$\log L_R = \xi_{RB} \log L_{\text{bol}} + \xi_{RM} \log M + b_R .$$

The bolometric luminosity of XRB is taken to be 5 times of the X-ray luminosity. For SMBH, the [OIII] line luminosity can be used as an estimate of the bolometric luminosity of the nuclear source. Different bolometric correction factors have been proposed by different authors.

Heckman et al. (2004) has reported the bolometric correction factor as $L_{\text{bol}}/L_{\text{OIII}} \sim 3500$, with a variance of 0.38 dex for uncorrected L_{OIII} . This relation was obtained

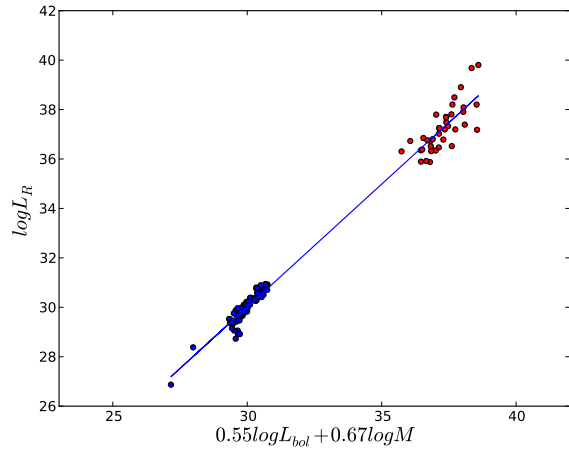
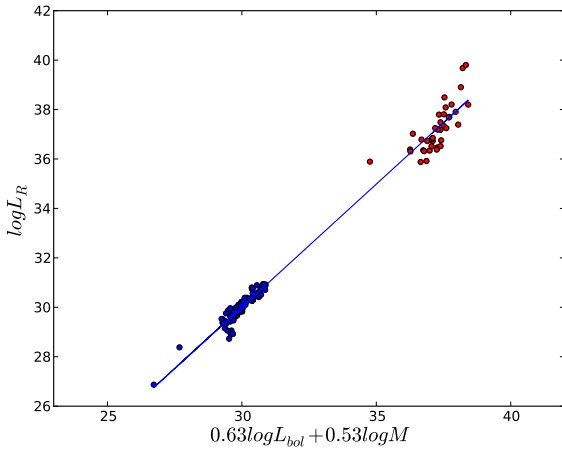
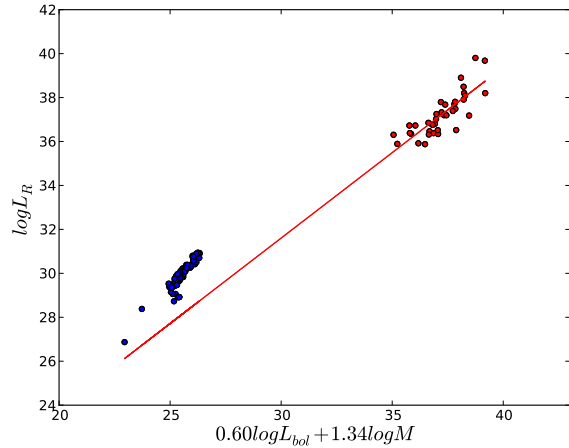
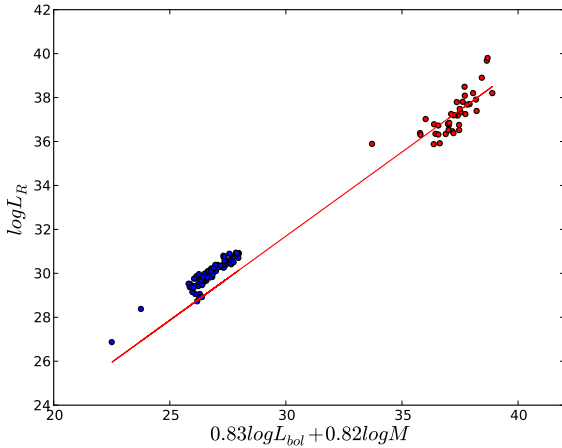


Figure 6. Projection of the Bolometric Fundamental Plane. In the top plot, SMBH sample is shown in red with the red solid line depicting the best-fit line for the SMBH sample. The XRB sample is put on the graph as blue dots without fitting. In the bottom plot, we show the combined fit for the complete sample including both the SMBH and the XRB sample. The blue line is the obtained best-fit line. Luminosities are given in erg/s while the masses are in the unit of solar mass.

using a sample dominated by powerful AGN ($L_{\text{OIII}} \sim 10^{6.5} - 10^9 L_{\odot}$). They have later extended the sample to lower luminosity AGN and have reported no evidence for systematic luminosity dependence on bolometric correction. But in a more recent study, Lamastra et al. (2009) has proposed bolometric correction factor to be luminosity dependent. The bolometric correction factor for extinction corrected [OIII] line luminosity is reported to be 87, 142 and 454 for [OIII] emission luminosity ranges of $\log L_{\text{OIII}}$ (in erg s^{-1}) = 38-40, 40-42, 42-44, respectively (Lamastra et al. 2009).

With these two conversions, we check for the best-fit coefficients for the SMBH sample only and find that while the bolometric luminosity obtained from the Heckman relation yields $\xi_{RB} = 0.83 \pm 0.4$ and $\xi_{RM} = 0.82 \pm 0.3$, the bolometric luminosity calculated with the Lamastra relation results in $\xi_{RB} = 0.60 \pm 0.14$ and $\xi_{RM} = 1.34 \pm 0.19$. A Kendall Tau correlation test verifies the statistical significance of the plane.

Figure 7. Same as Fig 5, but with Bolometric luminosity obtained from the relation proposed by L09 using extinction-corrected [OIII] luminosity.

For the former plane obtained with Heckman relation, we obtained a Kendall Tau coefficient value of $\tau = 0.56$ (with the probability for null hypothesis as $P_{\text{null}} \simeq 5.1 \times 10^{-7}$) while the plane obtained with Lamastra relation gives a Kendall Tau coefficient value of $\tau = 0.66$ ($P_{\text{null}} \simeq 2.8 \times 10^{-9}$).

Although a combined fit of the complete sample produces a bolometric fundamental plane relation, but individually the XRBs are incompatible with the bolometric plane stretched out by only the supermassive black holes (see Fig 5 and Fig 6), specially if the conversion of SMBH [OIII] luminosity to bolometric luminosity is obtained from extinction-corrected line luminosity using a luminosity-dependent conversion factor.

6 DISCUSSION

6.1 Recovering the Fundamental Plane of black hole activity

We recover the fundamental plane of black hole activity with our sample by converting the [OIII] line luminosities to respective X-ray luminosities in the 2-10 keV range. We use

Table 1. Recovering the Fundamental plane of black hole activity for the complete sample. The values reported are the parameters for the plane relation $\log L_R = \xi_{Ra} \log L_a + \xi_{RM} \log M$.

Plane	ξ_{RX}	ξ_{RM}	Kendall τ	P_{null}
Fundamental plane ($L_a = L_X$)				
Merloni et al. (2003)	0.60	0.78		
F Plane (H05)	0.64	0.61	0.872	$< 1 \times 10^{-10}$
F Plane (L09)	0.54	0.69	0.877	$< 1 \times 10^{-10}$
Plane in [OIII] ($L_a = L_{OIII}$)				
[OIII] Plane	0.83	0.82	0.67	1.3×10^{-9}
[OIII] ^c Plane	0.42	1.09	0.66	2.8×10^{-9}
Bolometric Plane ($L_a = L_{bol}$)				
B Plane (H05)	0.62	0.53	0.875	$< 1 \times 10^{-10}$
B Plane (L09)	0.54	0.67	0.872	$< 1 \times 10^{-10}$

two different approaches to convert the [OIII] line luminosities to X-ray (2-10 keV) luminosities - one using the H05 relation and the other using the L09 relation with extinction-corrected [OIII] luminosity. With both these approaches, we perform a combined fit of the supermassive and stellar black hole sample. We find that the plane parameters in both these cases agree to the fundamental plane of black hole activity, within the errors. The parameters for the planes obtained are reported in Table 1.

Using the H05 relation to do the necessary conversion, we also show that the stellar mass black holes completely agree to the best-fit plane of the supermassive sample when extrapolated to lower black hole mass range, even without fitting the stellar mass sample. The combined fit of both supermassive and stellar mass black hole (with H05 conversion) gives a plane

$$\log L_R = (0.64 \pm 0.4) \log L_X + (0.61 \pm 0.2) \log M .$$

The correlation coefficient found for low/hard state X-ray binaries ($\xi_{RX} \approx 0.7$) by Gallo et al. (2003) is consistent within the errors to the value obtained in our combined plane ($\xi_{RX} \approx 0.64$). This further strengthens our hypothesis that black holes of entire mass range follow these global plane parameters.

6.2 Discussing the Fundamental Plane in [OIII]

This study gives a relation between the [OIII] line luminosity of a galaxy hosting a supermassive black hole, its accretion rate and the mass of the black hole. The plane stretched in the 3D logarithmic space given by the radio and [OIII] luminosity as well as black hole masses follows the relations

$$\log L_R = (0.83 \pm 0.4) \log L_{[OIII]} + (0.82 \pm 0.3) \log M ,$$

$$\log L_R = (0.42 \pm 0.2) \log L_{[OIII]}^c + (1.09 \pm 0.2) \log M .$$

For radiatively inefficient accretion flow, as a first order approximation, analytical scaling of radio luminosity with mass accretion rate is empirically shown to be $L_R \propto \dot{M}^{1.4}$ (Blandford & Königl 1979; Falcke & Biermann 1995; Körtling et al. 2006). Using this relation, one can find a rough

dependence of [OIII] emission line luminosity on mass accretion for supermassive black holes as

$$L_{[OIII]} \propto \dot{m}^{1.68} M^{0.69} .$$

On the other hand, this study shows that the use of extinction-corrected [OIII] luminosity results in a much higher dependence on mass accretion, portraying a relation

$$L_{[OIII]}^c \propto \dot{m}^{3.33} M^{0.75} .$$

This relation is in agreement with previous studies showing that at low accretion rate, luminosity of an inefficient accretion structure has steep dependence on \dot{m} (Narayan et al. 1997; Mahadevan 1997). Recent studies also show that for accretion values lower than the critical value, the ionizing luminosity decreases $\propto \dot{m}^{3.5}$ (Sbarro et al. 2014).

6.3 Introducing a Bolometric fundamental plane

We also introduce a bolometric fundamental plane obtained by converting the corresponding [OIII] line luminosities to bolometric luminosities. Using a simple linear relation between [OIII] and bolometric luminosities (H05 method), we obtain a plane for the supermassive sample defined by the parameters $\xi_{RB} = 0.83 \pm 0.4$ and $\xi_{RM} = 0.82 \pm 0.3$. Inclusion of the XRBs to the SMBH sample does not change the parameters of the plane considerably. A projection of the plane obtained is shown in Fig 6.

When luminosity dependent bolometric correction factor (L09 method) is used to convert extinction-corrected [OIII] line luminosity to bolometric luminosity, we see that the parameters obtained for the plane are significantly different from the above-mentioned results. The bolometric luminosity obtained using the L09 conversion, depends on the mass accretion rate alone, with almost negligible dependence on black hole mass (see Fig 7). The relation is given by

$$L_{bol} \propto \dot{m}^{2.62} M^{0.20} .$$

This surprising negligible mass dependence might be explained as an effect of using luminosity-dependent bolometric correction factors. The bolometric correction factors reported in L09 increases for increasing [OIII] luminosity ranges, which might have effectively changed the mass scaling of bolometric luminosity. The dependency of bolometric luminosity in mass is suspected to be already included in the bolometric correction factor, which explains the negligible dependence of the resulting plane on black hole mass.

6.4 Radio-loudness in view of the Fundamental Plane

The Radio-loudness parameter is commonly defined as $R = L_{\nu R} / L_{\nu opt}$, where $L_{\nu R}$ and $L_{\nu opt}$ stand for the monochromatic luminosities at some specified radio and optical frequencies (Kellermann et al. 1989). Study of this parameter is crucial for addressing basic questions related to formation, acceleration and collimation of jets in different AGN classes. Various studies have shown that different classes of AGN have different Radio-loudness parameters, but whether the radio distribution is continuous or there is a radio bimodal-ity is still a matter of debate (eg. White et al. 2000). This

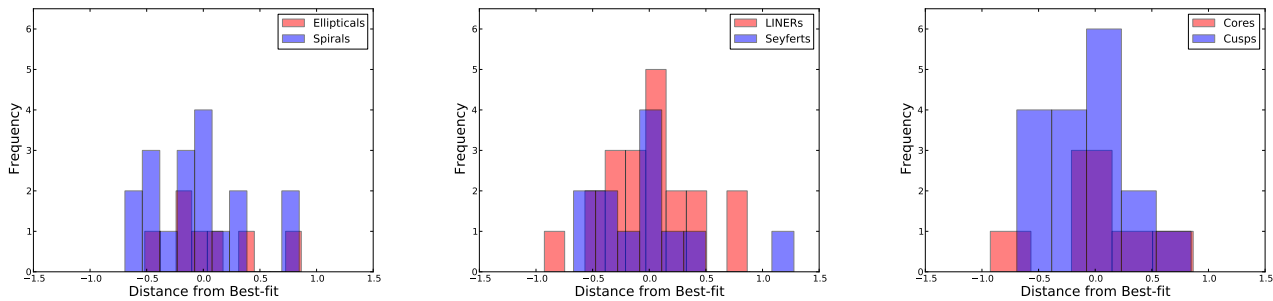


Figure 8. Distances of different classes of AGN from the best-fit plane

dichotomy has been used to infer different physical scenarios - some authors have proposed the spin paradigm, saying that more rapidly spinning black holes result in radio-loud AGNs (Blandford 1990; Wilson & Colbert 1995; Narayan & McClintock 2012) while some propose the magnetic flux paradigm, where the thin accretion disks give rise to radio-quiet AGN while hot (or thick) accretion disk are more efficient in depositing magnetic flux close to the black hole and hence give rise to radio-loud AGNs (Sikora et al. 2013).

The diverse sample of LLAGN used for the study follow one single Fundamental Plane equation, with no collective systematic deviation from the plane. As shown in Fig 8, where we have plotted histograms indicating the distances of the different sources from the best-fit plane, we see that no obvious differences can be spotted in the behavior of different AGN classes. Hence, the different types of LLAGN are consistent with having similar physical mechanisms to produce radio luminosity. In view of our plane, radio loudness is a general consequence of difference in Black hole masses - more massive black holes portraying more radio loud galaxies. Hence we suggest that the radio loudness parameter should not be used to infer different physical mechanisms in the sources.

We also perform the Kolmogorov-Smirnov (KS) test to quantify a distance between the empirical distribution functions of both the samples and check if different AGN samples come from the same distribution. We show using KS Statistics that the hypothesis that the underlying distributions of different AGN samples are identical can not be rejected.

6.4.1 Ellipticals and Spirals

We construct the fundamental plane separately for the ellipticals (sample - 7 ellipticals) and the spirals (sample - 18 spirals) and find the slopes to agree with each other within the uncertainties. A Kolmogorov-Smirnov (KS) test on the samples shows that the underlying distribution of the two samples are in agreement with being similar (KS statistics = 0.21, p-value = 0.95).

6.4.2 LINERs and Seyferts

By fitting the plane separately, we see that both the LINERs (sample - 20 LINERs) and Seyferts (sample - 12 seyferts) hold very similar Fundamental Plane relations. The histograms showing the deviation of these sources from the

fundamental plane can be seen in Fig 8. We also calculate the distances of the individual sources from the best-fit plane and compare the distribution functions of the LINERs and Seyferts. We see that both the types of AGN follow similar distribution functions. We get the KS statistics value as 0.25 and the p-value as 0.67. Hence, the hypothesis that the underlying distributions of the LINER and seyfert samples are identical can not be rejected.

6.4.3 Core, Sérsic and Double-Sérsic Galaxies

The brightness profile of the central regions of galaxies are described by the Nuker law (Lauer et al. 1995). Galaxies can be divided into two distinct classes according to their central brightness profile - the steep power law galaxies and the core galaxies with flattened slope. An alternate and more powerful description of this core/power-law dichotomy is based on inner logarithmic slope and is known as the Sérsic/core-Sérsic classification. The nuclei of core galaxies are considered to be radio-loud while those of cusp galaxies are radio-quiet (Capetti & Balmaverde 2006; Richings, Uttley & KÖrding 2011).

In our sample, we find that the core galaxies stretch out in a plane with a slope of 0.78, while both the Sérsic and double-Sérsic subsamples have similar slope of 0.95. It is interesting to compare the slight deviations in slope of the core and Sérsic subsamples as well as the elliptical and spiral subsamples. While both the ellipticals and the Sérsic samples has similar slopes of 0.7, both the spirals and the core galaxies has a higher slope of 0.9. A nonparametric KS test performed on the core and the cusp (Sérsic as well as double-Sérsic) galaxies showed that the underlying distribution of both the samples can be same (KS statistics = 0.27, p-value = 0.83).

7 CONCLUSION

We use a complete sample of 39 supermassive black holes selected from the Palomar Spectroscopic Survey and a selected sample of the best-studied stellar mass X-ray binaries, to study the general properties of accretion. We present results of multivariate regression analysis performed on the same and show that

- A fundamental plane of black hole activity is seen in the

logarithmic 3-dimensional space of black hole mass, radio luminosity and [OIII] emission line luminosity.

- The established fundamental plane of black hole activity in X-rays can be reproduced with this sample. It is possible to obtain the plane relation individually by the supermassive sample alone. On extrapolation to the lower mass black hole range, we see that the X-ray binaries agree to the plane stretched by the supermassive sample.

- We also introduce a bolometric fundamental plane for the supermassive sample, which does not completely agree to the complete sample after inclusion of the X-ray binaries. This plane shows negligible dependence on black hole mass, which might be due to the use of luminosity-dependent bolometric correction factor that effectively corrects for mass-scaling of bolometric luminosity.

- Finally, we look at the implication of the plane in radio-loudness of different AGN types. We see that after accounting for the non-linearity in the radio-[OIII] luminosity correlation and by including a mass scaling factor, we see no clear radio-dichotomy in the different types of AGN in our sample.

REFERENCES

- Akritas M. G., Siebert J., 1996, MNRAS, 278, 919
 Bianchi S., Guainazzi M., Matt G., Fonseca B. N., Ponti G., 2009, A&A, 495, 421
 Blandford R.D., Königl A., 1979, ApJ, 232, 34
 Blandford R. D., 1990, in *Active Galactic Nuclei*, ed. T. J.-L. Courvoisier & M. Mayor (Berlin: Springer), 161
 Capetti A., Balmaverde B., 2006, A&A, 453, 27
 Corbel S., Fender R.P., Tzioumis A.K., et al. 2000, A&A, 359, 251
 Corbel S., Körding E. & Kaaret P., 2008, MNRAS, 389, 1697-1702
 Corbel S., Coriat M., Brocksopp C., Tzioumis A.K., et al. 2013, MNRAS, 428, 25002515
 Coriat, M., Corbel, S., Prat L., et al., 2011, MNRAS, 414, 677
 Falcke H., Biermann P.L., 1995, A&A, 293, 665
 Falcke H., Malkan M.A. and Biermann P.L., 1995, A&A, 298, 375-394
 Falcke H., Körding E., Markoff S., 2004, A&A, 414, 895
 Fasano G., Vio R., 1988, *Newsletter of the Working Group for Modern Astronomical Methodology*, 7, 2
 Fender R. P., Corbel S., Tzioumis T., McIntyre, et al. 1999, ApJ, 519, L165
 Fender R. P., Belloni T. M., Gallo E., 2004, MNRAS, 355, 1105
 Gallo E., Fender R.P., Pooley G.G., 2003, MNRAS, 344, 60
 Gallo E., Fender R.P., Miller-Jones J. C. A., Merloni A. et al, 2006, MNRAS, 370, 13511360
 Gallo, E., Miller, B.P., & Fender, R. 2012, MNRAS 423, 590
 Gelino D. M., Harrison T. E., Orosz J. E., 2001, AJ, 122, 2668
 Heckman T. M., Kauffmann G., Brinchmann J., Charlot S., Tremonti C., White S.D.M., 2004, ApJ, 613, 109
 Heckman T. M., Ptak A., Hornschemeier A., Kauffmann G., 2005, ApJ, 634, 161 (H05)
 Heinz S., Sunayev R., 2003, MNRAS, 343, L59
 Ho L. C., Filippenko A. V., Sargent W. L., 1995, ApJS, 98, 477
 Ho L. C., Filippenko A. V., Sargent W. L. W., 1997 ApJS, 112, 315
 Ho L. C., Greene J. E., Filippenko, A. V., Sargent W. L. W., 2009, ApJS, 183, 1
 Hynes R. I., Steeghs D., Casares J., Charles P. A., O'Brien K., 2003, ApJ, 583, L95
 Jonker P., Nelemans G., 2004, MNRAS, 354, 355
 Kauffmann G., Heckman T. M., Tremonti C., Brinchmann J., et al., 2003, MNRAS, 346, 1055
 Kellermann K. I., et al. 1989, AJ, 98, 1195
 Körding E. G., Falcke H., Corbel S., 2006, A&A, 456, 439
 Körding E. G., Fender R.P., Migliari S., 2006, MNRAS, 369, 1451
 Körding E. G., Migliari S., Fender R.P. et al., 2007, MNRAS, 380, 301
 Lamastra A., Bianchi S., Matt G., et al. 2009, A&A, 504, 73 (L09)
 Lauer T.R., Ajhar E. A., Byun Y.-I., Dressler A., et al. 1995, AJ, 110, 2622
 Mahadevan R., 1997, ApJ, 447, 585
 McConnell N. J., Ma C.-P., Gebhardt K., Wright S. A., Murphy J. D., Lauer T. R., Graham J. R., Richstone D. O., 2011, Nature, 480, 215
 Merloni A., Heinz S., Matteo T.D., 2003, MNRAS, 345, 1057
 Merritt D., Ferrarese L., 2001, ApJ, 547, 140
 Nagar N. M., Falcke H., Wilson A. S., 2005, A&A, 435, 521
 Narayan R., Garcia M.R. and McClintock J.E., 1997, ApJ, 478, L79
 Narayan R. & McClintock J.E., 2012, MNRAS, 419, L69
 Osterbrock D. E., Ferland G. J., 2006, *Book Review: Astrophysics of Gaseous Nebulae and Active Galactic Nuclei*, 2edn
 Remillard R. A., McClintock J. E., 2006, ARA&A, 44, 49
 Richings A. J., Uttley P., and Körding E., 2011, MNRAS, 415, 2158
 Sbarrato T., Padovani P. and Ghisellini G., 2014, submitted in *Astro-ph*
 Shahbaz T., Naylor T., Charles P. A., 1994, MNRAS, 268, 756
 Shahbaz T., Bandyopadhyay R., Charles P.A. & Naylor T., 1996, MNRAS, 282, 977-981
 Sikora M. & Begelman M.C., 2013, ApJ, 764
 White R. L., Becker R. H., Gregg M. D., et al., 2000, ApJS, 126, 133
 Wilson A. S., & Colbert E. J. M., 1995, ApJ, 438, 62
 Zdziarski A. A., Gierliński M., Mikolajewska J., Wardziński G., Smith D. et al, 2004, MNRAS, 351, 791
 Zycki P. T., Done C., Smith D. A., 1999, MNRAS, 305, 231

This paper has been typeset from a \TeX / \LaTeX file prepared by the author.

APPENDIX A: MAIN PROPERTIES OF THE SAMPLE

Table A1. SMBH Sample : Main properties

Name	Mass (in M_{\odot})	L_R (in erg/s)	L_{OIII} (in erg/s)
NGC5033	2.89523e+07	2.92753e+36	7.46678e+39
NGC4138	1.48166e+07	2.24663e+36	1.04037e+39
NGC3998	1.8723e+09	1.59028e+38	1.62112e+40
NGC2655	6.18073e+07	2.1361e+37	1.24977e+40
NGC5353	1.43127e+09	1.59777e+38	5.13102e+38
NGC5354	2.65312e+08	6.24036e+37	3.26808e+38
NGC4278	6.72349e+08	5.04692e+37	4.76834e+38
NGC3226	3.51531e+08	1.76814e+37	3.60821e+38
NGC4419	2.32308e+07	6.07591e+36	1.99971e+40
NGC4486	3.43764e+09	4.78596e+39	3.51229e+39
NGC5846	7.61949e+08	3.05999e+37	4.26385e+38
NGC2273	4.30474e+07	2.45978e+37	1.63045e+41
NGC6500	2.77027e+08	8.01106e+38	1.45928e+40
NGC3190	1.42429e+08	2.40036e+36	3.49149e+38
NGC5363	3.75418e+08	1.22118e+38	1.53139e+40
NGC3147	3.16161e+08	8.10255e+37	1.79206e+40
NGC3628	1.50039e+06	7.79999e+35	1.06867e+37
NGC3627	4.43963e+07	7.55398e+35	1.11365e+39
NGC7743	3.14113e+06	5.34024e+36	3.14872e+40
NGC4169	1.2373e+08	1.51898e+37	4.93036e+41
NGC3169	1.44378e+08	1.57809e+37	2.65927e+39
NGC4203	1.22352e+08	5.34512e+36	1.46688e+37
NGC4293	1.01086e+07	2.41945e+36	2.05736e+39
NGC4374	1.00496e+09	3.1004e+38	1.08288e+39
NGC4579	1.44378e+08	4.77634e+37	3.26039e+39
NGC7479	5.235e+07	1.56935e+37	4.76577e+40
NGC5377	8.40809e+07	1.78146e+37	2.21031e+39
NGC4548	1.06744e+07	2.0253e+36	7.56412e+37
NGC4258	2.40533e+07	8.29525e+35	1.34388e+39
NGC3607	4.19661e+08	3.31531e+36	2.11336e+39
NGC5866	8.25699e+07	1.04987e+37	3.29625e+38
NGC4216	1.81405e+08	2.19408e+36	4.72302e+38
NGC4589	3.67869e+08	6.40442e+37	2.34894e+39
NGC4565	7.16962e+07	2.08178e+36	7.39625e+38
NGC1167	2.95376e+08	6.34151e+39	1.27083e+41
NGC3945	1.5611e+08	6.35733e+36	3.65437e+38
NGC2787	1.86646e+08	7.07416e+36	6.76e+37
NGC4143	2.2071e+08	5.70298e+36	1.0395e+38
NGC4636	3.26608e+08	3.28353e+36	1.07745e+38

Table A2. XRB Sample : Main properties

Name	Mass (in M_{\odot})	L_R (in erg/s)	L_X (in erg/s)
GX 339-4	0.85	30.2947	36.8804
GX 339-4	0.85	30.2964	36.8865
GX 339-4	0.85	30.2214	36.4579
GX 339-4	0.85	30.2253	36.3264
GX 339-4	0.85	29.6867	35.7584
GX 339-4	0.85	29.8308	36.2568
GX 339-4	0.85	30.2596	36.8415
GX 339-4	0.85	30.2748	36.8639
GX 339-4	0.85	30.07	36.1511
GX 339-4	0.85	30.0423	36.1014
GX 339-4	0.85	30.385	36.5264
GX 339-4	0.85	29.6798	35.7412
GX 339-4	0.85	30.4414	37.0319
GX 339-4	0.85	30.3732	36.8019
GX 339-4	0.85	29.9292	36.1871
GX 339-4	0.85	29.5174	35.104
GX 339-4	0.85	30.2887	36.6635
GX 339-4	0.85	29.6657	35.9521
GX 339-4	0.85	29.6163	35.8259
GX 339-4	0.85	29.4217	35.541
GX 339-4	0.85	29.6243	35.8174
GX 339-4	0.85	29.06	35.6163
GX 339-4	0.85	29.3822	35.2641
GX 339-4	0.85	29.3753	35.088
GX 339-4	0.85	29.6282	35.5829
GX 339-4	0.85	29.6359	35.5467
GX 339-4	0.85	29.06	35.3753
GX 339-4	0.85	29.5274	35.03
GX 339-4	0.85	30.0483	36.1957
GX 339-4	0.85	30.0028	36.0686
GX 339-4	0.85	30.2204	36.2061
GX 339-4	0.85	29.7352	35.8662
GX 339-4	0.85	29.8547	35.9808
GX 339-4	0.85	29.8209	35.9521
GX 339-4	0.85	29.986	36.0798
GX 339-4	0.85	30.9233	37.6382
GX 339-4	0.85	30.8729	37.623
GX 339-4	0.85	29.1511	35.2263
GX 339-4	0.85	29.6163	35.7472
GX 339-4	0.85	30.5381	37.099
GX 339-4	0.85	30.4988	37.1011
GX 339-4	0.85	30.5906	37.1851
GX 339-4	0.85	30.6183	37.2245
GX 339-4	0.85	30.7215	37.3335
GX 339-4	0.85	30.7749	37.4036
GX 339-4	0.85	30.8725	37.4639
GX 339-4	0.85	30.9385	37.4921
GX 339-4	0.85	30.9243	37.5183
GX 339-4	0.85	30.858	37.5309
GX 339-4	0.85	30.2596	36.5293
GX 339-4	0.85	30.4135	37.243
GX 339-4	0.85	30.7031	37.6152
GX 339-4	0.85	30.5066	37.37
GX 339-4	0.85	29.361	35.1534
GX 339-4	0.85	29.428	35.3232
GX 339-4	0.85	29.4694	35.7376
GX 339-4	0.85	29.3232	35.2818
GX 339-4	0.85	29.3537	35.2818
GX 339-4	0.85	29.9558	36.2818
GX 339-4	0.85	30.1014	36.4486
GX 339-4	0.85	29.8133	36.0078
GX 339-4	0.85	29.8133	36.1416
GX 339-4	0.85	29.8308	35.9911

Table A3. ... continued

Name	Mass (in M_{\odot})	L_R (in erg/s)	L_X (in erg/s)
GX 339-4	0.85	29.8108	35.9843
GX 339-4	0.85	30.3661	36.5224
GX 339-4	0.85	28.729	35.4783
GX 339-4	0.85	29.9877	35.8689
GX 339-4	0.85	30.1027	36.0331
GX 339-4	0.85	30.1683	36.1914
GX 339-4	0.85	30.1925	36.2972
GX 339-4	0.85	30.2312	36.3931
GX 339-4	0.85	30.9112	37.5736
GX 339-4	0.85	30.9078	37.5395
GX 339-4	0.85	30.9173	37.5294
GX 339-4	0.85	29.7034	35.6692
GX 339-4	0.85	29.8259	35.7647
XTE J1118+480	1	28.92	35.57
XTE J1118+480	1	28.92	35.46
XTE J1118+480	1	28.92	35.47
XTE J1118+480	1	28.92	35.45
XTE J1118+480	1	28.92	35.56
V404 Cyg	1	30.5637	36.7929
V404 Cyg	1	28.3794	32.4075
V404 Cyg	1	30.5782	36.7841
V404 Cyg	1	30.2842	36.4424
V404 Cyg	1	30.7422	36.7018
V404 Cyg	1	30.0895	36.0074
V404 Cyg	1	30.8014	36.6908
V404 Cyg	1	29.872	35.2893
V404 Cyg	1	30.173	36.0732
V404 Cyg	1	30.1151	36.0067
V404 Cyg	1	30.3491	36.5397
V404 Cyg	1	30.3839	36.2693
V404 Cyg	1	30.0851	35.922
V404 Cyg	1	30.0939	36.0506
V404 Cyg	1	30.571	36.7517
V404 Cyg	1	30.8932	36.9999
V404 Cyg	1	29.7566	35.1663
V404 Cyg	1	29.9631	35.4186
V404 Cyg	1	30.24	36.1864
V404 Cyg	1	30.7613	36.7581
AO6200	1.04	26.87	30.85